Supporting Information

Immobilizing Nanozymes on 3D printed Metal Substrates for Enhanced Peroxidase-like Activity and Trace-level Glucose Detection

Paramita Koley,[a] Ranjith Kumar Jakku[a], Tayebeh Hosseinnejad[a], Selvakannan Periasamy[a], and Suresh K. Bhargava*[,a]

[a]Centre for Advanced Materials & Industrial Chemistry (CAMIC), School of Applied Sciences, RMIT University, GPO Box 2476, Melbourne 3001, Australia.
Corresponding Authors: Suresh K Bhargava; Email: suresh.bhargava@rmit.edu.au

Experimental section:

Chemicals and materials:

$Fe(NO_3)_3 \cdot 9H_2O$ (99%), benzene 1,4-dicarboxylic acid (95%), and peroxidase substrates such as TMB, ABTS, and OPD were purchased from Sigma-**A**ldrich. These chemicals are directly used in the reaction without purification. The de-ionized water was collected from a Millipore Autopure system.

Synthesis of MIL 88B: 12.12 g of ($Fe(NO_3)_3.9H_2O$) was dissolved in 75 ml DMF by stirring 500 rpm in a Schott bottle. Separately, H_2BDC (4.98 g) and DMF (75 ml) were added in a 250 ml Teflon liner under the same stirring speed. Both solutions were stirred for 15 min at room temperature. Then ($Fe(NO_3)_3.9H_2O$) solution was added to the H_2BDC precursor solution. 12 ml NaOH solution (4.0 M) was added dropwise to the Fe and H_2BDC solution mixture and stirred again for 30 min at room temperature. The Teflon liner was placed in an autoclave and heated to 100 °C for 24 h. After cooling the reaction mixture to room temperature, the reddish-brown product was isolated by washing with DMF followed by methanol. The MIL 88B (MOF) is formed.

Synthesis of degraded/thermally treated MOF: After the synthesis of MOF (MIL 88B), it is treated in different temperatures such as 400, 450, 500 and 550 °C in argon atmosphere. Depending on degradation temperature, the nanozymes are named as DEG 400, DEG 450, DEG 500 and DEG 550.

Synthesis of MIL 88B deposited 3D printed substrates: 3D printed metallic substrates have been used which is the composition of Ti, V, and Al alloy. The substrates were calcined at 500 °C for 3h in air for calcination. During the synthesis of MOF (MIL 88B), calcined 3D printed substrate was placed in the autoclave. After the synthesis, the substrates were washed with

DMF and MeOH and then dried in a 60 ℃ oven for overnight. Then MIL 88B deposited 3D printed substrates had been synthesized.

Synthesis of DEG 500 deposited 3D printed substrate: After the deposition of MIL 88B on 3D printed substrate, the substrate was treated at 500 ℃ temperature for 4h in an argon atmosphere in a tubular furnace. The images of fresh 3D printed metal substrates and the DEG 500 deposited 3D printed metal substrates are shown in Figure 11.

Characterization instruments:

Powder X-ray diffractograms (P-XRD) were collected on a Bruker AXS diffractometer (D8 ADVANCE) with a Cu anode (Kα radiation, λ = 1.5406 Å) and data was recorded in the 2Θ range from 10 to 90° in a continuous scanning mode with 0.01° sampling pitch and 5° min^{-1} scan rate. Transmission electron micrographs (TEM) images of the catalysts were captured at 100 kV on a JEOL 1010 TEM. High-resolution transmission electron microscopy (HR-TEM) images and selected area electron diffraction (SAED) pattern were collected at 200 kV voltage on a JEOL 2010 TEM. The morphology of the catalysts was investigated using a Scanning Electron Microscope. (FEI Verios 460L field-emission scanning electron microscope (FESEM) containing an ultrahigh resolution Schottkey emitter SEM). S-2 Energy-dispersive X-ray analysis (EDS) was performed on same instrument equipped with an Oxford X-MaxN 20 EDXS detector with an accelerating voltage of 25 kV. X-ray photoelectron spectroscopy (XPS) were investigated on a Thermo Scientific K-Alpha instrument (monochromatic Al Kα radiation, Ephoton = 1486.6 eV). The binding energy (B.E) in each case, that is, core levels and valence band maxima were corrected using an internal reference peak of C 1 s peak centered at 284.8 eV. Confocal Micro-Raman spectra recorded at room temperature in the range of 200–1200 cm-1 using Horiba Jobin–Yvon Lab Ram HR spectrometer with a 17 m internal He–Ne (Helium– Neon) laser source of excitation wavelength of 632.8 nm. The powder catalyst (about 5–10 mg) were usually spread onto a glass slide below the confocal microscope for Raman measurements. The BET surface area, pore volume and pore sizes were determined by using the N2 adsorption-desorption method using BEL Sorb II Instruments, Japan at liquid nitrogen temperature. Before the measurement the samples were degassed at 110 °C for 5 h. Then BET analysis is performed in liquid nitrogen atmosphere for over-night. FT-IR spectrums of catalysts were investigated on a DIGILAB (USA) IR spectrometer. The electrochemical behaviour of MIL 88B and DEG 500 was assessed using CV in a three-electrode system. A combination of 10 µL of MIL 88B and DEG 500 was amalgamated with 90 µL of an acetone solution. Subsequently, 30 µL of this blend was deposited onto a refined glassy carbon

electrode, which, after drying, served as the operational electrode. The Ag/AgCl electrode functioned as the reference, while a platinum wire was the counter electrode. The investigative solution was a 0.2 M sodium acetate buffer with a pH of 3.6. The CV parameters included a voltage range of 1.5 V to -1.5 V, a step size of 10 Mv, a current range of 10 µA, and a scan rate (ν) of 50 mV/sec.

Standard assay for the peroxidase catalytic activity study:

To evaluate the enzymatic activities of the MIL88B and its series of degradants, such as DEG 400, DEG 450, DEG 500, and DEG 550, were performed at 25 °C. In a standard procedure, the 20.4 µL (100 mM) H_2O_2 was added to the 100 µg/mL catalysts and 97 µL (800 µM) TMB as a substrate in a reaction volume containing 200 µL of sodium acetate buffer (100 mM, pH~4). Additionally, the enzymatic activities of the catalysts were also investigated against OPD (600 µM) and ABTS (600 µM) substrates as a part of the selectivity study. This typical calorimetric reaction involves the oxidation of substrates by H_2O_2 in the presence of a catalyst, according to Equation 1. The TMB substrate's corresponding UV-vis absorption band at 653 nm was measured continuously within 10 minutes using the MIL88B, DEG 400, DEG 450, DEG 500, and DEG 550 catalysts. By varying incremental concentrations of the DEG 500 catalyst (20, 40, 60, 80, 100, 120, and 140 µg/mL), the absorbance of the TMB substrate was also measured.

Moreover, the steady-state kinetic experiments of the TMB were conducted using 100 µg of DEG 500 catalyst with a fixed concentration of H_2O_2 (100 mM) and incremental concentrations of the TMB substrate (200, 400, 600, 800, and 1000 µM). In the same way, the kinetic study with a fixed concentration of TMB substrate (800 µM) and varying concentrations of H_2O_2 (20, 40, 60, 80, 100, and 150 mM) was also performed using 100 µg of DEG 500 catalyst.

$$\text{Substrate (TMB, ABTS, ODP)} + \text{catalyst} + H_2O_2 \longrightarrow \text{oxidized substrate} + H_2O \qquad (1)$$

The kinetic parameters were calculated using Lineweaver–Burk plots of the double reciprocal of the Michaelis– Menten equation as described below

$$\frac{1}{V} = \frac{K_m}{V_m}\left(\frac{1}{[S]} + \frac{1}{K_m}\right) \qquad (2)$$

where V is the initial velocity, V_m represents the maximal reaction velocity, [S] corresponds to the substrate concentration, and K_m is the Michaelis–Menten constant.

The pH dependence studies were conducted using various pH buffer solutions (100 mM, pH 1.0–10.0). The buffers used in the study were glycine–HCl buffer (pH 1.0–2.0), acetate buffer (pH 3.0–5.0), phosphate buffer (pH 6.0–8.0), and Tris-HCl buffer (pH 9.0–10.0). Temperature dependence studies were also done from 15 to 85 °C for the DEG 500 catalyst by maintaining the above conditions. Furthermore, the stability of DEG 500 in different pH buffers at different temperatures was determined by incubating the DEG 500 in different buffer solutions at different temperatures, respectively, for a period of 24 h and the peroxidase-like catalytic activity experiments were carried out under optimized conditions (pH 4.0, 25 °C).

1.2. Colorimetric detection of glucose

The process for detecting glucose was described in the following manner.

A solution of glucose with concentrations ranging from 1 μM to 5 mM was combined with phosphate-buffered saline (100 mM PBS, pH 7.4) containing 100 μL of glucose oxidase (GOx) with a concentration of 2 mg mL^{-1}. The resulting solution with a total volume of 200 μL, was incubated at a temperature of 37°C for 30 minutes. Following incubation, the solution was mixed with 600 μL of acetate buffer (100 mM, pH 4), 150 μL of TMB (1.2 mM), and 50 μL of DEG 500(2 mg mL^{-1} in acetate buffer). After another 10-minute incubation at 37 °C, the absorbance at 653 nm was measured. In control experiments, 100 μL of 1 mM glucose, 5 mM fructose, and 5 mM sucrose were used for a comparison purpose. To determine glucose levels in spiked foetal bovine serum (4 mM glucose), apple juice, and grape juice, the samples were initially centrifuged at 12,000 rpm for 40 minutes. The resulting supernatants were diluted by factors of 50, 2500, and 5000, respectively, using 100 mM PBS buffer (pH 7.4) for the subsequent experiment.

DFT Calculations:

We firstly optimized the structure of Fe(II)-H_2O_2, Fe(III)-H_2O_2, Fe(II)-TMB, and Fe(III)-TMB molecular models to determine the transition states and their energy barriers on the reaction energy profile. The corresponding cartesian coordinates of atoms in the optimized structures of our obtained Fe(II)-H_2O_2, Fe(III)-H_2O_2, Fe(II)-TMB, and Fe(III)-TMB molecular models have been reported in Table S4. Geometry optimization was carried out using the B3LYP/6-31G* level of theory. It should be mentioned that B3LYP, a widely employed density functional theory (DFT) method, stands for Becke's three-parameter hybrid functional in

combination with Lee, Yang, and Parr's correlation functional. The Becke three-parameter exchange functional incorporates non-local exchange correlation, while the LYP correlation functional is a non-empirical function that includes the gradient correction [1]. The harmonic frequency analysis was used to confirm that the found structures correspond to transition states with one imaginary frequency. All calculations were performed using GAMESS suite of programs[2]. We performed QTAIM topological analysis of electron density and its derivatives using the obtained B3LYP/6-311G** wave functions for all optimized structures as input by AIM2000[3]. All calculated QTAIM properties for iron active site models have been listed in Table S5.

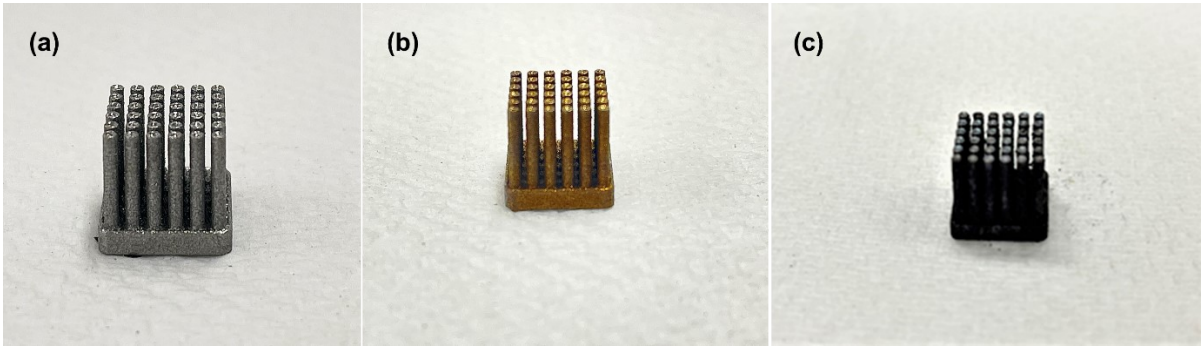

Figure S1: (a) fresh (b) calcined and (c)DEG 500 deposited 3D printed Ti-Al-V substrates.

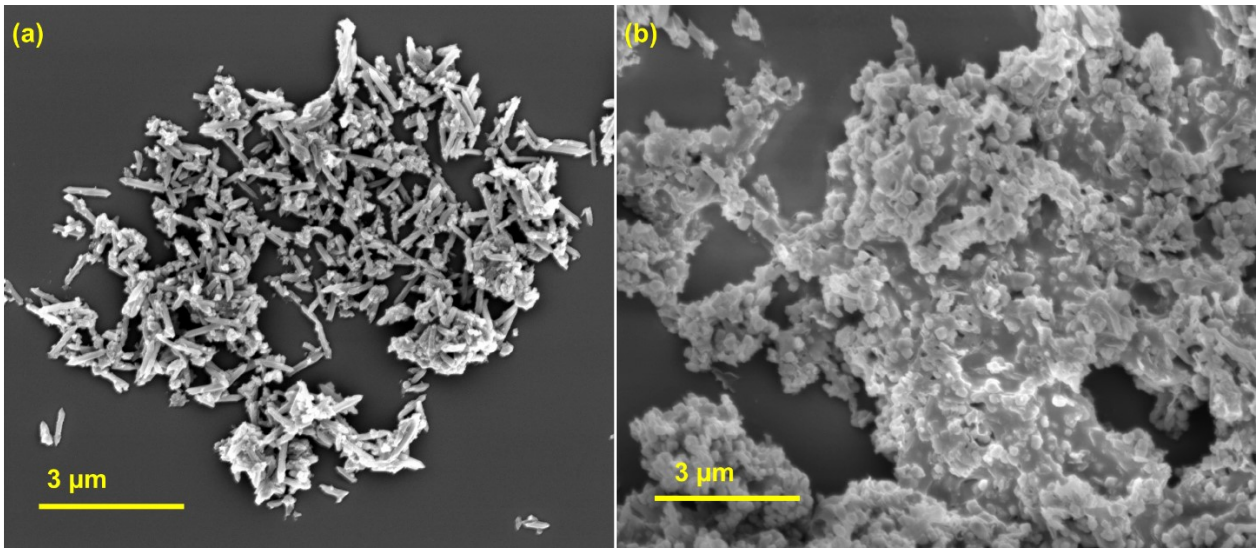

Figure S2: (a)SEM images of MIL88B and (b) DEG 500

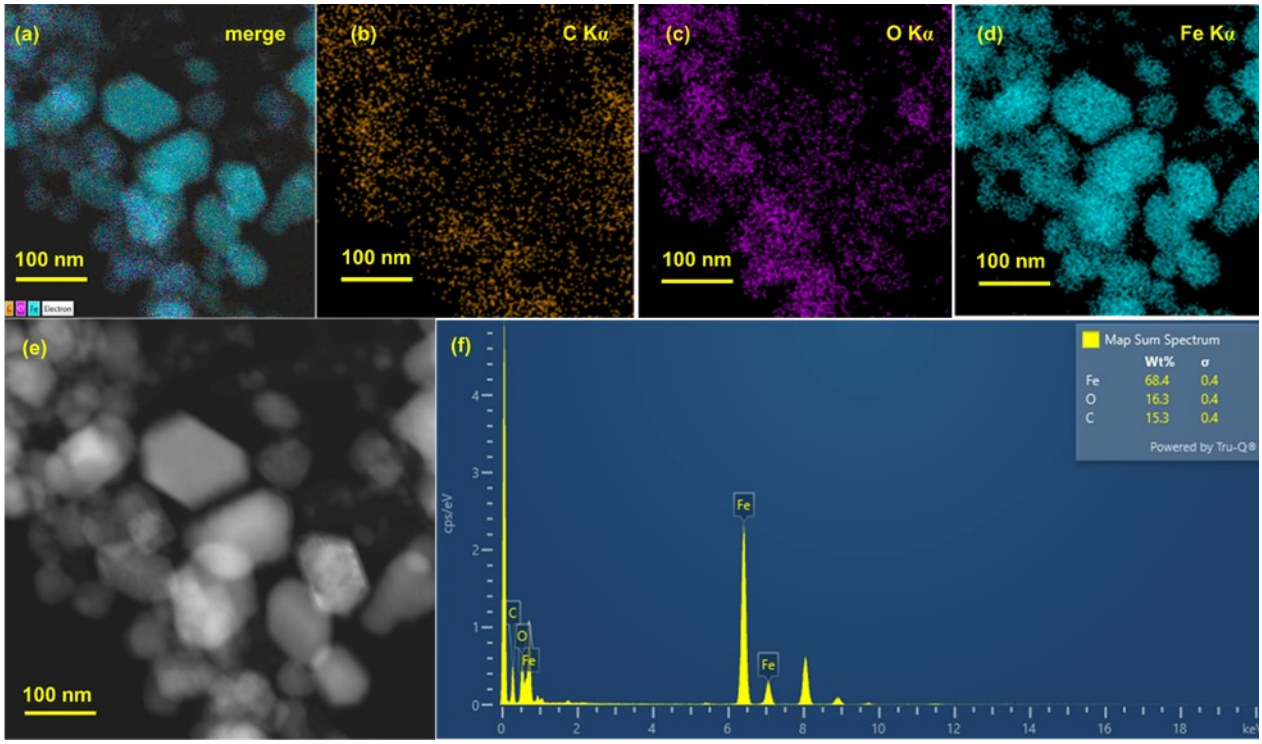

Figure S3: TEM-EDX images of (a)-(e) of DEG 500 nanozyme and (f) EDX spectra of DEG 500 nanozyme

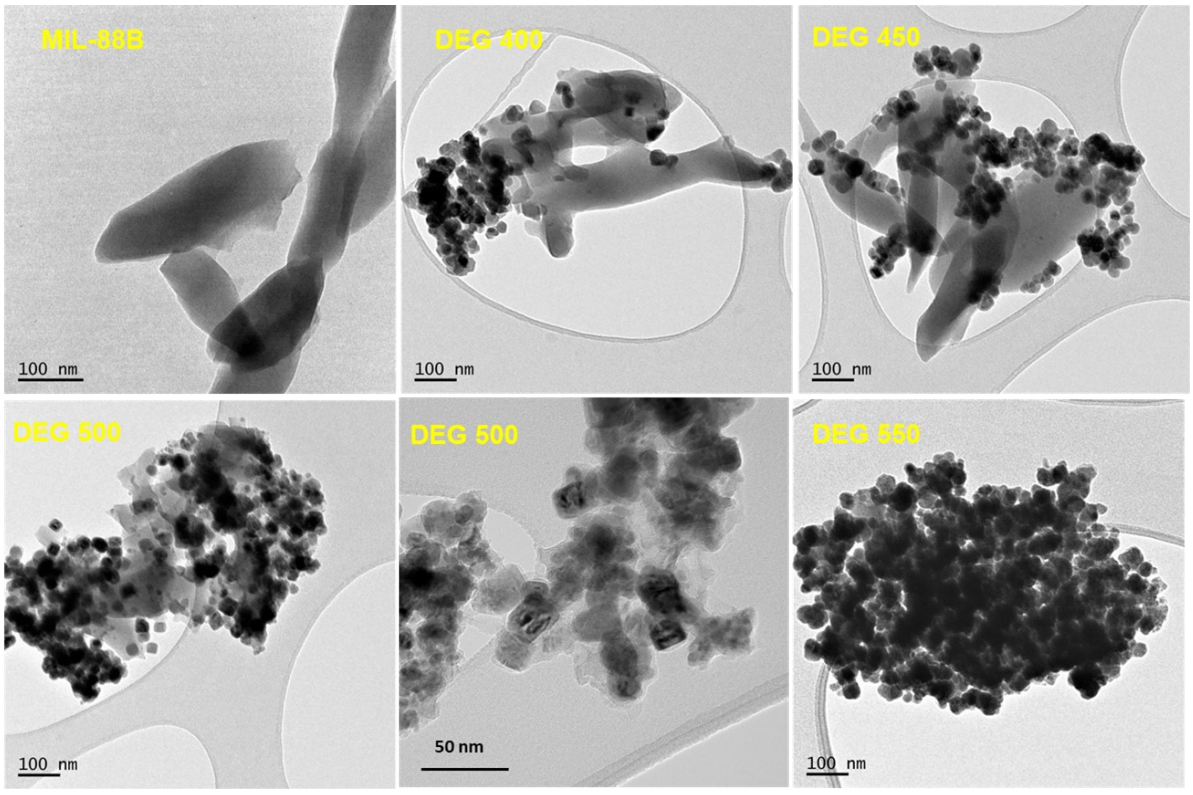

Figure S4: TEM images of different nanozymes

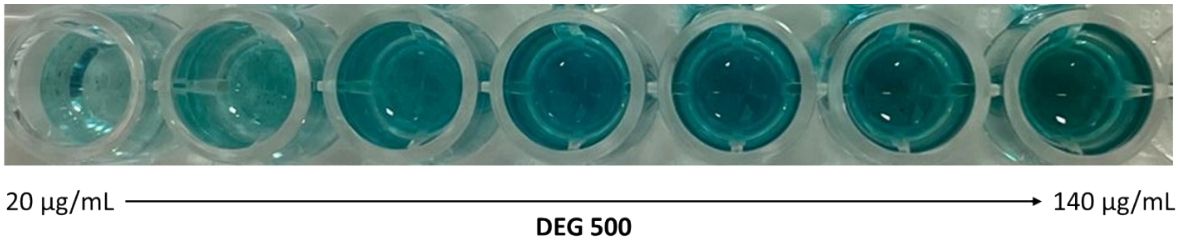

Figure S5: Increasing intensity of color upon incremental concentrations of DEG 500 (20-140 µg/mL)

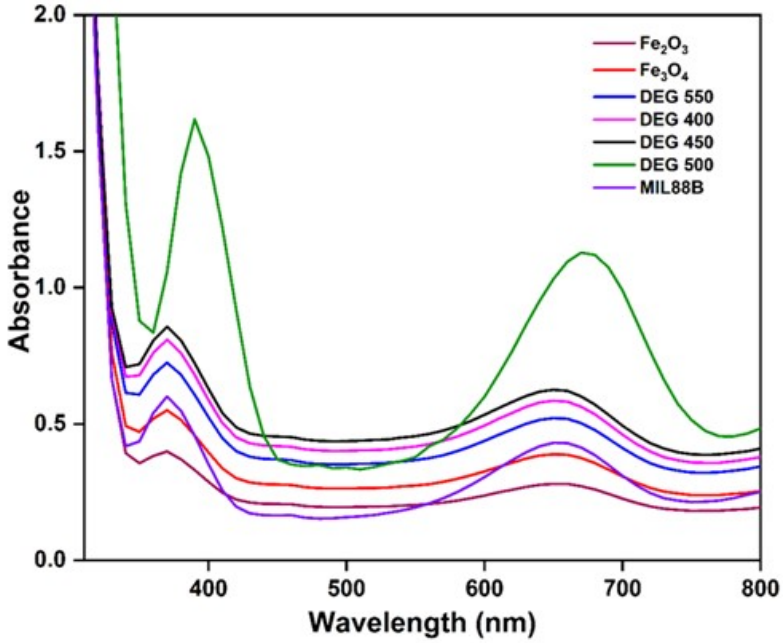

Figure S6: Nanozyme activity of different catalysts

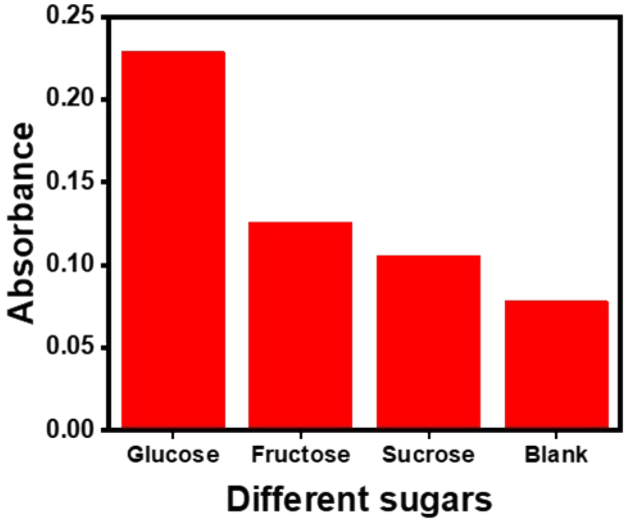

Figure S7: The selectivity of glucose detection with 5 mM fructose, 5 mM lactose, and 1 mM glucose.

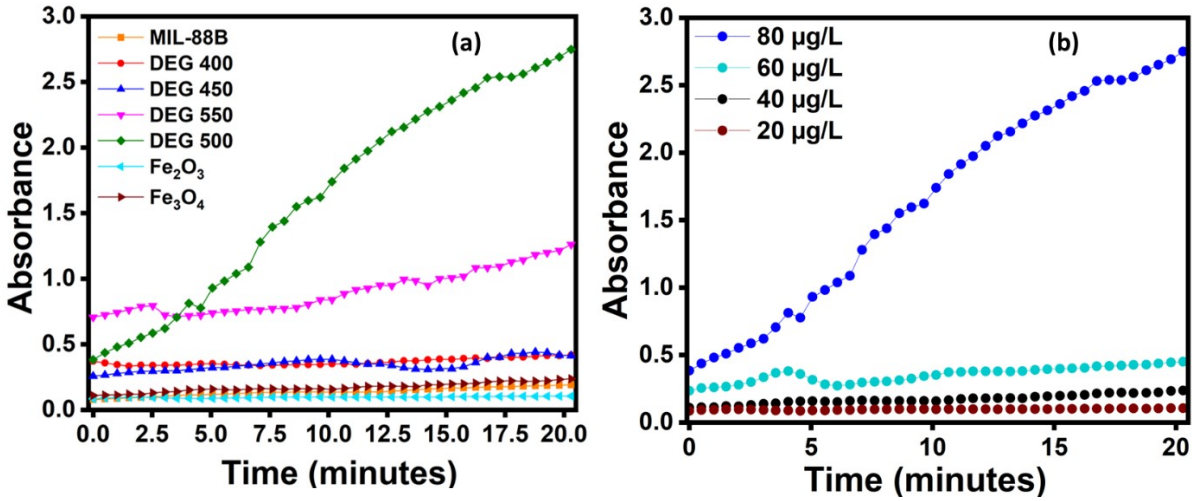

Figure S8: (a) Absorbance curves of TMB substrate oxidation as a function of time for different nanozyme. The absorbance at 653 nm was measured in a reaction mixture of 100 mM acetate buffer (pH 4), 800 mM TMB and 100 mM H_2O_2 over various nanozyme and (b) absorbance curve of TMB substrate oxidation (time dependent kinetics) for different concentration of DEG 500 nanozyme.

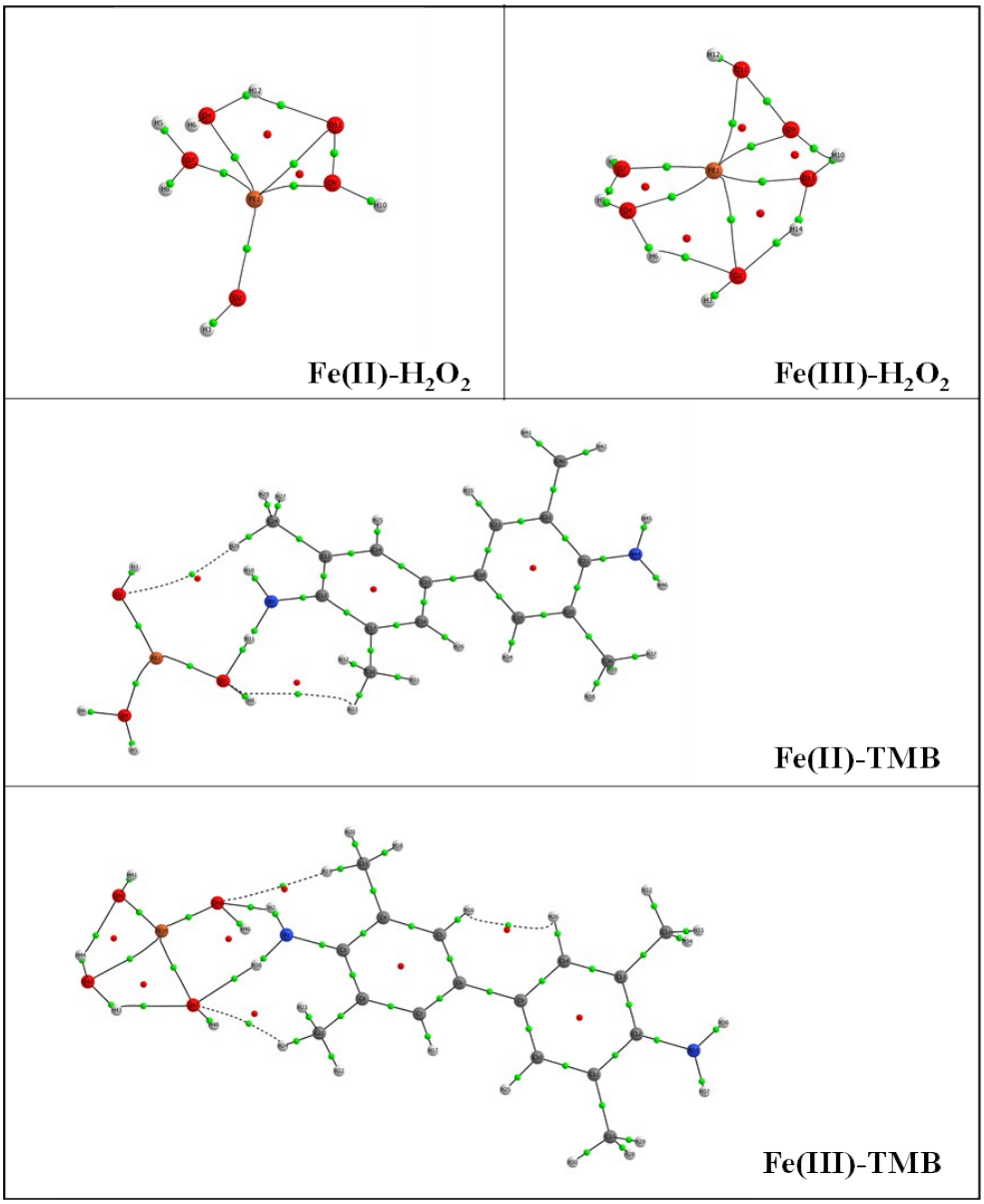

Figure S9: QTAIM graphs of Fe(II)-H_2O_2, Fe(III)-H_2O_2, Fe(II)-TMB, and Fe(III)-TMB active site molecular models, obtained by the analysis of B3LYP/6-311G** electron density functions. Bond Critical Points: Green circles; Ring Critical Points: Red circles; Bond Paths: Gray solid and dashed lines.

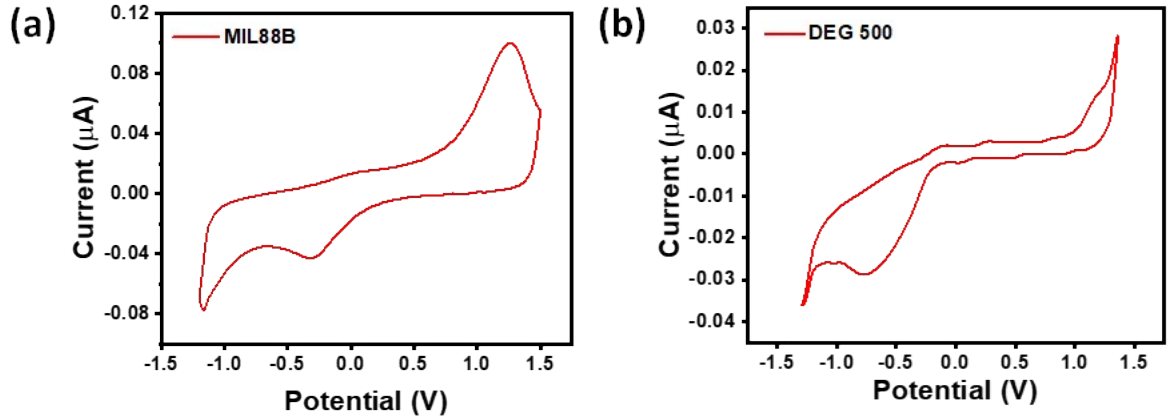

Figure S10: The CV curves of (a) MIL 88B and (b) DEG 500 in sodium acetate buffer solution, at scanning rate is 50 mV/s.

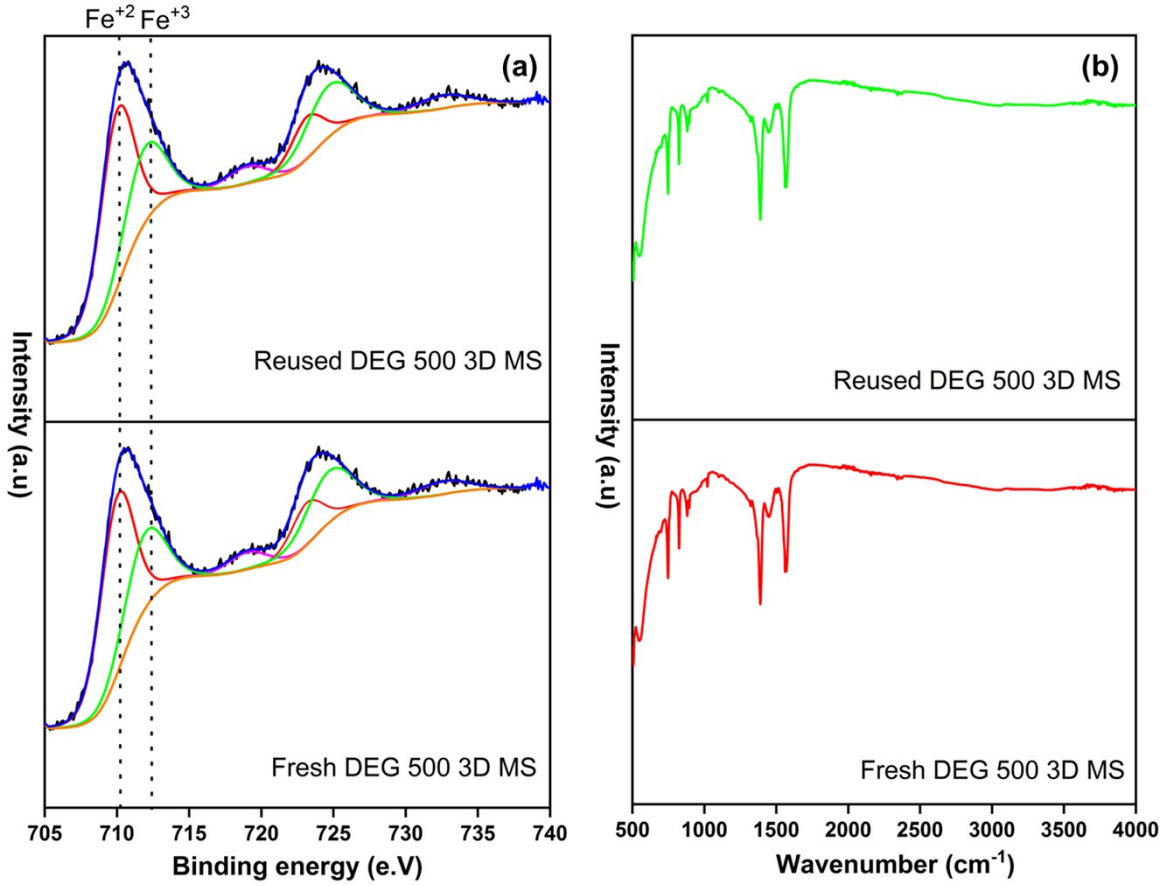

Figure S11: (a) XPS and (b) FT-IR of the fresh and reused DEG 500 3D MS nanozyme.

Table S1: BET surface area, average pore volume and diameter.

Catalyst	S_{BET} (m^2g^{-1})	Pore volume (cm^3g^{-1})	Pore diameter (nm)
MIL88B	346.6	0.346328	12.6
400	139.9	0.210804	11.5
450	101.5	0.157155	11.4
500	80.3	0.103160	14.3
550	47.1	0.088255	14.8

Table S2: Surface percentage (from XPS) of different oxygen species

Catalyst	**Oxygen vacancy (%)**	**Lattice oxygen (%)**	**-OH group (%)**
500	56.8	25.4	17.8
550	50.1	38.7	11.2
450	39.5	46.1	14.4
400	39.1	45.8	15.1
MIL88B	38.5	45.6	15.9

Table S3: Surface percentage of different Fe species

Catalyst	**Fe^{+2} (relative %)**	**Fe^{+3} (relative %)**
500	61.2	38.8
550	34.6	65.4
450	50.7	49.3
400	36.8	63.2

MIL88B	31.3	68.7

Table S4: The cartesian coordinates of atoms in the optimized structure of Fe(II)-H_2O_2, Fe(III)-H_2O_2, Fe(II)-TMB, and Fe(III)-TMB active site molecular models in transition state, calculated at B3LYP/6-31G* level of theory.

Fe(II)-H_2O_2

Atom	Atomic number	Cartesian coordinates (XYZ)		
Fe	26.0	-0.38036	-3.61055	-0.18915
O	8.0	0.62073	-4.24490	-1.58120
H	1.0	0.44931	-4.56673	-2.46967
O	8.0	-1.33600	-4.49456	1.38494
H	1.0	-2.79107	-4.14491	-0.36099
H	1.0	-0.90031	-5.22763	1.83307
O	8.0	-2.22129	-3.65068	-0.96218
H	1.0	-2.44131	-3.79377	-1.88761
O	8.0	0.88601	-3.11248	1.31220
H	1.0	1.62183	-2.49503	1.22873
O	8.0	-0.36128	-2.24170	1.29666
H	1.0	-1.19834	-3.64498	1.87790

Fe(III)-H_2O_2

Atom	Atomic number	Cartesian coordinates (XYZ)		
Fe	26.0	-0.50664	-3.59847	-0.10156
O	8.0	0.32324	-5.08312	-1.14617
H	1.0	-0.22239	-5.36572	-1.89889
O	8.0	-1.54113	-5.22366	0.81686
H	1.0	-2.22226	-4.84521	0.17269

H	1.0	-0.91894	-5.76482	0.29792
O	8.0	-2.31402	-3.66620	-0.82352
H	1.0	-2.70018	-3.21444	-1.57901
O	8.0	0.91136	-3.04262	1.23482
H	1.0	1.43460	-2.43524	-0.68217
O	8.0	-0.31423	-2.13438	1.33586
H	1.0	-0.68544	-2.36753	2.19600
O	8.0	0.87484	-2.68870	-1.43423
H	1.0	0.95249	-3.69359	-1.56459

Fe(II)-TMB

Atom	**Atomic number**	**Cartesian coordinates (XYZ)**		
Fe	26.0	-2.44805	-7.99653	2.48846
O	8.0	-4.23282	-7.77731	2.36309
H	1.0	-4.59232	-6.89012	2.40237
O	8.0	-1.68474	-9.78995	2.43811
H	1.0	-0.88958	-9.80406	2.98325
H	1.0	-2.35173	-10.36833	2.83986
O	8.0	-1.13397	-6.72820	2.71111
H	1.0	-0.34403	-6.83934	2.18769
N	7.0	-2.06287	-5.02577	1.56958
H	1.0	-3.00401	-4.80829	1.78929
H	1.0	-1.62130	-5.76143	2.16590
C	6.0	-1.45366	-4.60497	0.40051
C	6.0	-2.13178	-4.69898	-0.82489
C	6.0	-1.52995	-4.26138	-1.99029
C	6.0	-0.23508	-3.74041	-2.00312
C	6.0	0.43872	-3.66753	-0.78476
C	6.0	-0.14426	-4.07981	0.40744
C	6.0	0.40340	-3.28223	-3.27680
C	6.0	1.78379	-3.33222	-3.45994
C	6.0	2.39541	-2.91167	-4.63359

C	6.0	1.61733	-2.41489	-5.69876
C	6.0	0.21918	-2.36034	-5.52693
C	6.0	-0.35440	-2.78679	-4.33644
C	6.0	-3.53361	-5.28694	-0.86336
H	1.0	-2.07254	-4.35396	-2.90860
H	1.0	1.42705	-3.25152	-0.75301
H	1.0	-3.87206	-5.40165	-1.88944
H	1.0	-3.55629	-6.26234	-0.38267
H	1.0	-4.23262	-4.63107	-0.34613
C	6.0	0.64931	-3.95743	1.70100
H	1.0	1.38866	-3.16382	1.62120
H	1.0	-0.00437	-3.73807	2.53749
H	1.0	1.17510	-4.89078	1.90417
H	1.0	2.40173	-3.72592	-2.67636
H	1.0	-1.41908	-2.71240	-4.22865
C	6.0	3.90862	-3.00521	-4.75335
H	1.0	4.33769	-2.02058	-4.92774
H	1.0	4.34249	-3.40392	-3.83935
H	1.0	4.18533	-3.66476	-5.57340
C	6.0	-0.67991	-1.82781	-6.63196
H	1.0	-1.72338	-1.86089	-6.32773
H	1.0	-0.42872	-0.79440	-6.86209
H	1.0	-0.57254	-2.42954	-7.53225
N	7.0	2.21472	-1.98927	-6.89131
H	1.0	1.67473	-1.63218	-7.64991
H	1.0	3.20202	-2.02848	-7.02628

Fe(III)-TMB

Atom	**Atomic number**	**Cartesian coordinates (XYZ)**		
N	7.0	0.16906	0.47086	-0.22002
H	1.0	-0.41620	-0.17105	-0.72707
C	6.0	-0.15645	1.79615	-0.20901

C	6.0	-1.44657	2.22814	-0.55751
C	6.0	-1.74076	3.57495	-0.57283
C	6.0	-0.80880	4.54702	-0.22064
C	6.0	0.45625	4.10075	0.15488
C	6.0	0.79608	2.76437	0.15302
C	6.0	-1.15251	5.99526	-0.26326
C	6.0	-0.18989	6.97376	-0.48692
C	6.0	-0.49957	8.32085	-0.53989
C	6.0	-1.82508	8.73647	-0.39932
C	6.0	-2.81103	7.77177	-0.18488
C	6.0	-2.46128	6.43726	-0.10162
C	6.0	-2.49897	1.19078	-0.90004
H	1.0	-2.72071	3.87243	-0.89257
H	1.0	1.19788	4.81066	0.46807
H	1.0	-3.40998	1.66794	-1.24327
H	1.0	-2.16095	0.49766	-1.66217
H	1.0	-2.73701	0.59772	-0.02041
C	6.0	2.17950	2.29688	0.56242
H	1.0	2.83409	3.14169	0.74632
H	1.0	2.12178	1.70149	1.46965
H	1.0	2.62767	1.66334	-0.19611
H	1.0	0.82973	6.68141	-0.64034
H	1.0	-3.23380	5.72349	0.10227
C	6.0	0.59205	9.35127	-0.75874
H	1.0	0.43747	9.90525	-1.68190
H	1.0	0.62463	10.06344	0.06211
H	1.0	1.56062	8.87193	-0.82007
C	6.0	-4.26166	8.19195	-0.04434
H	1.0	-4.89160	7.32782	0.12351
H	1.0	-4.39964	8.87373	0.79075
H	1.0	-4.61396	8.68556	-0.94756
N	7.0	-2.15637	10.08388	-0.46558

H	1.0	-3.10534	10.37418	-0.44157
H	1.0	-1.47325	10.76313	-0.70469
H	1.0	1.13634	0.19629	-0.34702
Fe	26.0	1.12841	-2.18315	-1.45365
O	8.0	1.34971	-3.38445	-0.00510
H	1.0	1.04898	-3.31001	0.90520
O	8.0	2.96820	-3.12728	-1.82389
H	1.0	3.29618	-2.20881	-1.68589
H	1.0	2.77255	-3.53226	-0.94033
O	8.0	-0.40487	-1.40574	-2.27386
H	1.0	-0.31748	-0.56005	-2.73597
O	8.0	2.38923	-0.68733	-1.39816
H	1.0	2.32312	-0.08209	-2.15242

Table S5. QTAIM properties of some selected key bond critical points (BCPs) and ring critical points (RCPs) in Fe(II)-H_2O_2, Fe(III)-H_2O_2, Fe(II)-TMB, and Fe(III)-TMB active site molecular models, which calculated via wave function analysis at B3LYP/6-311G** level of theory.

	ρ_b	$\nabla^2\rho_b$	V_b	G_b	H_b	$\lvert V_b\rvert/G_b$
Fe(II)-H_2O_2						
BCPs						
Fe-O9	0.0752	0.387	-0.1149	0.1058	-0.0091	1.0860
Fe-O11	0.0780	0.3872	-0.1186	0.1077	-0.0109	1.1012
O9-O11	0.2237	0.1304	-0.3306	0.1816	-0.149	1.8204
RCPs						
Fe-O11-O9	0.0670	0.3425	-0.1029	0.0942	-0.0087	1.0923
Fe(III)-H_2O_2						
BCPs						
Fe-O9	0.0715	0.3849	-0.1162	0.1062	-0.01	1.0941
Fe-O11	0.0663	0.3520	-0.1073	0.0976	-0.0097	1.0993
O9-O11	0.2298	0.1529	-0.3185	0.1783	-0.1402	1.7863
RCPs						
Fe-O11-O9	0.0639	0.3230	-0.0980	0.0894	-0.0086	1.0961
Fe-O9-H10-O13	0.0236	0.0135	-0.0220	0.0239	0.0019	0.9205
Fe(II)-TMB						
BCPs						
Fe-O7	0.1150	0.7660	-0.2164	0.2039	-0.0125	1.0613

O7-H11	0.0356	-0.0065	-0.2999	0.1491	-0.1508	2.0114
N9-H11	0.2954	-1.3115	-0.3016	0.0972	-0.2044	3.1028
N9-H10	0.3541	-1.8167	-0.2736	0.0697	-0.2039	3.9253
RCPs						
Fe-O2-H28-C24-C13-C12-N9-H11-O7	0.0026	0.0084	-0.0009	0.0015	0.0006	0.6000
O7-H11-N9-C12-C17-C30-H33	0.0041	0.0177	-0.0025	0.0035	0.001	0.7142
Fe(III)-TMB						
BCPs						
Fe-O47	0.0829	0.5445	-0.1389	0.1375	-0.0014	1.0101
O47-H38	0.1660	0.0982	-0.0283	0.0264	-0.0019	1.0719
N1-H38	0.3377	-1.8123	-0.2408	0.0538	-0.1870	4.4758
N1-H2	0.3460	-1.8567	-0.2262	0.0560	-0.1702	4.0392
RCPs						
Fe-O47-H38-N1-H2-O45	0.0102	0.0486	-0.0074	0.0098	0.0024	0.7551
O47-H38-N1-C3-C8-C21-H24	0.0081	0.0297	-0.0048	0.0061	0.0013	0.7868

References:

1. A. D. Becke, *The Journal of chemical physics*, 1993, **98**, 1372-1377.
2. M. Gordon, J. Jensen, S. Koseki, N. Matsunaga, K. Nguyen, S. Su and T. Windus, *J. Comput. Chem*, 1993, **14**, 1347-1363.
3. R. Bader, *McMaster University, Hamilton, Canada*, 2000.